Iğdır Üniversitesi Fen Bilimleri Enstitüsü Dergisi, 11(2): 1068-1079, 2021
Journal of the Institute of Science and Technology, 11(2): 1068-1079, 2021

ISSN: 2146-0574, eISSN: 2536-4618

Fizik / *Physics* **DOI: 10.21597/jist.828194**

Araştırma Makalesi / *Research Article*

Geliş tarihi / Received: 20-11-2020 **Kabul tarihi / Accepted: 06-02-2021**

Atıf İçin: Candan İ, 2021. Hidrojen Moleküllerinin v = 1 Durumuna Raman Uyarılması. Iğdır Üniversitesi Fen Bilimleri Enstitüsü Dergisi, 11(2): 1068-1079.

To Cite: Candan I, 2021. Raman Excitation of Hydrogen Molecules to v = 1 State. Journal of the Institute of Science and Technology, 11(2): 1068-1079.

Raman Excitation of Hydrogen Molecules to v = 1 State

İlhan CANDAN [1*]

ABSTRACT: Coherent anti-Stokes Raman scattering (CARS) can reveal a molecule's vibrational spectrum to a great extent. Instantaneous interaction of Stokes and pump beams stemming from powerful pulsed lasers excites a molecule's vibrational modes in CARS. In this technique, combining two visible laser beams could create spectra resonances relating to vibrational transitions. In this work, Raman excitation of Hydrogen molecules to v = 1 state is achieved by CARS spectroscopy. CARS measurements are successfully carried out for H_2 S-branch and Q-branch transitions using our laser system. This measurement proves the feasibility of CARS experiment which could be employed to excite molecules to a specific rovibrational state. Moreover, experiments conducted for CARS signal with respect to various gas pressures differing between 200 and 600 torr for S-branch transition of H_2 molecule.

Keywords: H2, Coherent anti Stokes Raman scattering, S-branch, Q-branch

[1] İlhan CANDAN (**Orcid ID:** 0000-0001-9489-5324), Dicle Üniversitesi, Fen Fakültesi, Fizik Bölümü, Diyarbakır, Türkiye

***Sorumlu Yazar/Corresponding Author:** İlhan CANDAN, e-mail: ilhan.candan@dicle.edu.tr

Bu çalışma İlhan CANDAN'nın Yüksek Lisans tezinden üretilmiştir. Makale 14-17 Kasım 2018 tarihlerinde Diyarbakır'da düzenlenen "The 3rd International Engineering and Natural Sciences Conference 2018 (IENSC 2018)" kongresinde sözlü olarak sunulmuştur.

INTRODUCTION

Terhune and Maker first observed coherent anti-Stokes Raman scattering (CARS)(Maker & Terhune, 1965; Terhune & Maker, 1963). Non-linear Raman processes is one of such spectroscopic technique which has been feasible with employment of lasers. Spontaneous Raman (Anderson, 1971; Buric et al, 2009; Farahani & Gogolla, 1999; Tang et al, 2020), Resonance Raman(Kiefer & Bernstein, 1972; Liu et al, 2013; Saito et al, 2003; Xie et al, 2009), Inverse Raman(Takaya et al, 2019; Yeung, 1974), Hyper Raman scattering(Babenko et al, 2020; Madzharova et al, 2017; Verdieck et al, 1970; Zhu et al, 2018) and Raman-induced Kerr effect(Ando et al, 2020; Heiman et al, 1976; Kakinuma & Shirota, 2018) are amongst various examples of Raman processes. CARS is a very effective non-linear spectroscopic technique that has been used in various applications such as temperature and concentration measurements, molecular relaxation processes, gas-phase and plasma diagnostics and femtosecond chemistry(El-Diasty, 2011; Lempert & Adamovich, 2014; Tolles et al, 1977; Zheltikov, 2000). CARS spectroscopy has been a common means of detection for modern optical experiments and comprehensively mentioned in literature(Christensen et al, 2019; Eckbreth, 1996; Eesley, 2013; Harvey & Nibler, 1978; Jiang et al, 2020; Kifer, 1980; Short et al, 2015; Yan et al, 2018; Yang et al, 2018).

CARS is very promising for its potential to obtain analytical and spectroscopic knowledge relating to Raman active resonances in matter including gas, liquid and solid(Jones et al, 2019; Kushwaha et al, 2018; Portnov et al, 2010). CARS is generally used in applications such as in chemistry, physics, and related fields to determine a structural fingerprint through which molecules can be identified. CARS is also employed for species selective microscopy and combustion diagnostics by exploiting the selectivity of vibrational modes(Cutler et al, 2018; Ehn et al, 2017; Goodhead et al, 2015; Zhang & Cheng, 2018). In this technique, combining two visible laser beams could create spectra resonances relating to vibrational transitions. CARS exhibits a third-order non-linear process. Compared to second-order non-linear effect, it can be applied to both an isotropic and a non-centrosymmetric medium. Additionally, it has a conversion efficiency for coherently producing photons that are significantly greater than spontaneous Raman scattering (CARS can achieve 10^5 increase in efficiency of conversion (Begley et al, 1974)). That is a very practical tool to obtain luminescent samples' spectra such as electric discharges, impurities, fluorescent materials and combustion systems as well as some solutes(Butler et al, 2016; Dedic et al, 2017; Sarri et al, 2019; Teramoto & Ono, 2014; Tolles et al, 1977). Because of advantages mentioned above, in this paper, we employ CARS technique for experimentally determining the pump wavelength that will be used in the Stimulated Raman Pumping (SRP) scheme(Candan, 2016).

In CARS, two laser fields with ω_1 and ω_2 frequencies mix in a medium in order to produce a non-linear polarisation that oscillates at $2\omega_1 - \omega_2$ frequency since it is an optical phenomenon that is coherent and third order non-linear process. This is resonantly enhanced when $\omega_1 - \omega_2$ frequency difference coincides with a Raman active transition in the active sample as displayed in Figure 1. ω_1 and ω_2 are corresponding to ω_{pump} and ω_{Stokes} fields, respectively. The resulting field produced at $2\omega_1 - \omega_2$ required to match in phase with non-linear polarisation produced by pump field in ω_1 and ω_2 frequencies. This process is described according to following expression:

$$2k(\omega_1) - k(\omega_2) = k(2\omega_1 - \omega_2). \quad (1)$$

The wave vector mismatch Δk becomes finite because of material dispersion(Ochkin, 2009; Regnier et al, 1974). Additionally, dispersion rate in dilute gases becomes very low. The rotation-vibration resonances' coherence length in Hydrogen molecule happens to be $\approx$ 10 cm for a collinear geometry(Regnier et al, 1974).

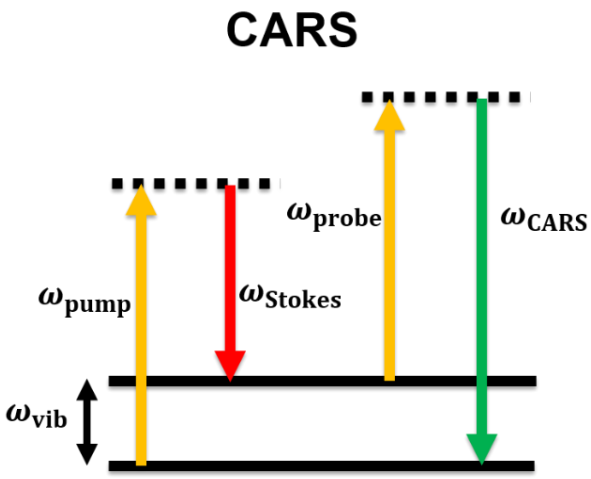

Figure 1. Energy levels of CARS is demonstrated. This process is a coherent and non-linear optical phenomenon of third order where ω_{pump} and ω_{Stokes} combine through a medium to produce a signal with frequency of $2\omega_{pump} - \omega_{Stokes}$. The resultant signal is resonantly improved once $\omega_{pump} - \omega_{Stokes}$ coincide with vibrational constant of energy levels.

The CARS process needs two high-powered (commonly pulsed) laser fields that have ω_p and ω_s frequencies which are tightly focused into sample. Therefore, owing to non-linear mixing of two laser beams, an output beam is generated in the medium that is coherent and similar to a moderate intensity laser beam at frequency $\omega_{as} = 2\omega_p - \omega_s$. The efficiency rate of frequency ω_{as} strongly depends on the present molecular resonances at a frequency difference that equals to $\omega_p - \omega_s$, the laser power, the number density of species and the resonance line width(Kliewer et al, 2012; Tolles et al, 1977).

CARS wavelength calculation

In the Raman Spectrum, vibrations and rotations of molecules are in visible rage. Molecules including H_2 , N_2 or O_2 can be studied only with Raman spectroscopy as their rotations and vibrations happens to be infra-red inactive. Raman active molecules needs to follow rules of selection for Raman spectrum. Raman spectroscopy happens to be two-photon phenomenon. For vibrational transitions, the selection rules follow $\Delta v = \pm 1$ in the Raman spectrum, in which Stokes transitions are corresponding to $\Delta v = +1$, and anti-Stokes transitions to $\Delta v = -1$. Moreover, that obey $\Delta J = 0, \pm 2$ for the rotational transitions in which the S-branch, Q-branch and O-branch transitions are labelled as $\Delta J = +2$, $\Delta J = 0$ and $\Delta J = -2$, respectively.

In this paper, wavelength of CARS is determined in H_2. For calculating CARS wavelength in H_2, S-branch transition is selected. This occurs from $v'' = 0$, $J'' = 1$ to $v' = 1$, $J' = 3$. $v'' = 0$, $J'' = 1$ quantum state is selected since at the room temperature it is the most populated state. For this particular transition, vibrational constant (ω_{vib}) is equal to 4712.91 cm^{-1} $(\overline{v_v})$ (Dabrowski, 1984; Turner et al, 1977). In our calculations, the wavenumber units are employed in terms of frequency. Initially, we established the Stokes laser (IR laser) wavelength. Therefore, the wavelength of Stokes line is determined to be at 1064.555 nm. Utilizing expression of $\overline{v_p} = \overline{v_v} + \overline{v_s}$, in which v_v and v_s are assigned to pump and Stokes wavenumbers, respectively. After that, $\overline{v_p} = 14106.51\ cm^{-1}$ could be determined. Next, wavelength of CARS could be determined using $\overline{v_{cars}} = \overline{v_v} + \overline{v_p}$ expression. Thus, that enable us to calculate $\overline{v_{cars}} = 18819.42\ cm^{-1}$ as illustrated in Figure 2.

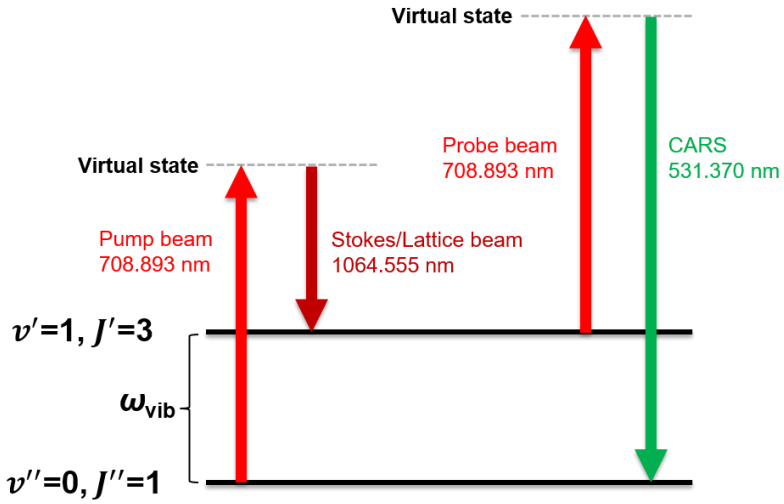

Figure 2. Figure shows CARS process in H_2 molecules. 708.893 nm pump beam stimulates the H_2 at $v'' = 0$, $J'' = 1$ to another level(virtual). After that, 1064.555 nm Stokes beam instantaneously brings the molecule down to a rovibrationally excited state of $v' = 1$, $J' = 3$. Next, 708.893 nm probe beam excites it to another nonreal state once more. Finally, because it does not remain in this nonreal state, the molecule spontaneously must deexcite to the ground state together with releasing 531.370 nm CARS photon.

Moreover, wavelength of CARS signal is determined for Hydrogen molecule's Q-branch transition that stems from $v'' = 0$, $J'' = 1$ level and reaches to $v' = 1$, $J' = 1$. Scattering rate is related to polarisability tensor of the transition squared(Eckbreth, 1996). Scattering intensity of Q-branch is greater than S-branch because the scattering intensity is related to the Placzed-Teller coefficients of each transition. Therefore, Q-branch transition's CARS signal is much higher compared to S-branch. Vibrational constant equals to 4155.25 cm^{-1} for this transition and the corresponding wavelengths are determined. Thus, if we apply 1064.555 nm Stokes beam, then 738.07 nm resulting pump beam can be determined. Therefore, 564.84 nm CARS signal occurs in the measurement.

MATERIALS AND METHODS

Experimental setup

In order to conduct CARS experiment, two laser beams need to be employed. Pump and Stokes beam are generated using a dye laser (Continuum, ND6000, USA) and custom-made laser (Continuum, USA), respectively. For realizing the experiment, we need to both spatially and temporally coincide these two beams in a H_2 containing glass cell.

Laser system

Dye laser

Dye laser is used to produce pump beam in the experiment. This laser is injected using pulsed laser comprising Nd:YAG crystal as gain medium (Quanta-Ray Pro-series, Spectra-Physics) that contains 532 nm frequency doubled output and has a repetition rate of 10 Hz. In order to produce the necessary tunable output of the dye laser (700 to 740 nm wavelength rage), 114 mg L^{-1} and 20 mg L^{-1} dye solution of LDS 750 in methanol were employed for oscillator and amplifier, respectively. Thus, necessary tunable 719 nm output was generated.

IR laser (Custom-built)

IR laser beam is employed to be Stokes beam in the experiment. For optical Stark acceleration/deceleration, a high-energy, chirped laser has explicitly constructed and built at UCL (Coppendale et al, 2011; Maher-McWilliams et al, 2012). The laser system consists of two pulsed

outputs. It is primarily originated in a laser of 1064 nm Nd:YVO_4 microchip which could quickly tune the frequency using a cavity containing an electro-optic crystal. A laser diode is injection-locked the output and a fibre amplifier is used to magnifies the output to 1 W power. Next, the resultant beam is splitted into separate pulses employing pulse shaper. Later, generated pulses are separated and then connected to separate fibres in which one of them is 55 m longer compared to other one. The resultant difference in path generates 275 ns time delay. Once the microchip laser is being chirped, that produces a frequency variation which is well-defined. After exiting fibres, two pulses are magnified using different flash lamp stages and high intensities are produced using pulsed Nd:YAG amplifiers. Such laser system can produce two high power beams that have flat-top temporal shapes. In this system, the frequency change can be chirped by 1.1 GHz during the pulse of 140 ns(Coppendale et al, 2011). Prior to the experiment, wavemetre (HighFinesse GmbH, WS-6, Germany) and Burleigh wavemetre (WA- 2000, USA) are employed to calibrate ND6000 and custom-built laser wavelength, respectively.

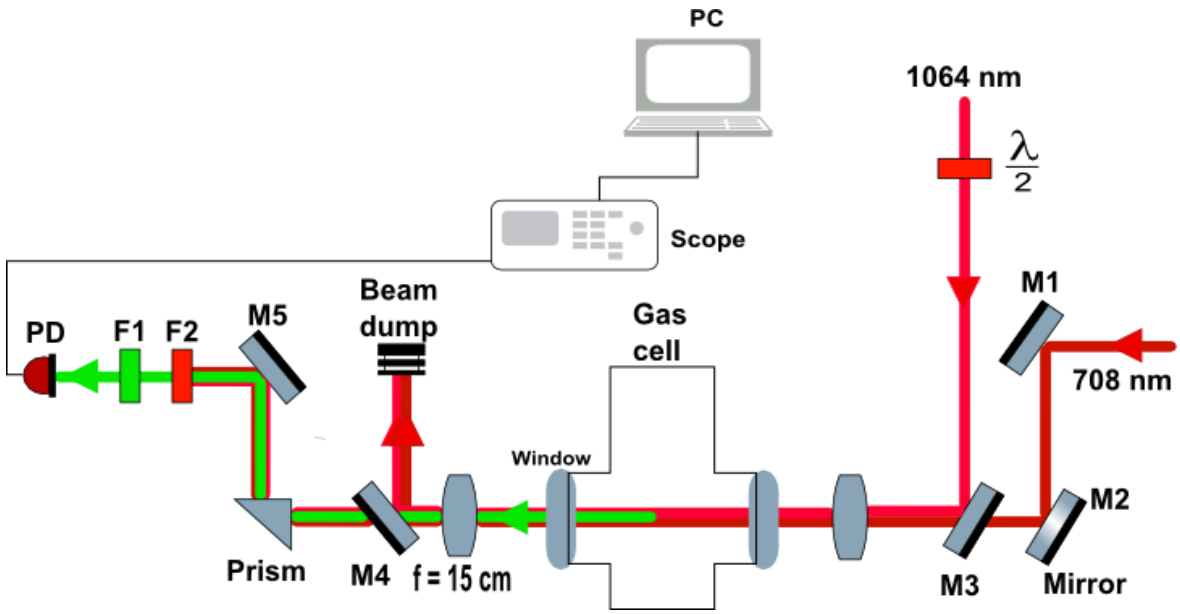

Figure 3. Experimental setup of CARS in H_2 molecule is demonstrated. 708.893 nm pump beam and 1064.555 nm Stokes beam are nearly co-propagating as well as being spatially and temporally intersected in a gas cell containing H_2. The resultant green beam is displayed and identified employing a PD while filtering remaining pump and Stokes beams is achieved.

Optical layout

Optical setup of CARS experiment is demonstrated in Figure 3. Experiment contains different laser beams that are nearly co-propagating. 1064 nm IR beam is utilized as Stokes beam. 708 nm dye laser beam is employed as pump beam. Because linearly polarising pump and Stokes beams are very important(Bartlett et al, 2008), a $\lambda/2$ plate is positioned in path of Stokes beam for parallel polarization. Once two fields possess same polarisation, output signal could be significantly improved. 15 cm lens is used for focusing two collinear beams into gas cell. Following the intersection of beams being spatial and temporal overlapped, a green colour CARS signal is produced as illustrated in Figure 3. For separating the resultant beam, a few additional optics are utilized. Another 15 cm lens is employed for collimating the beams at the end of the gas cell. M4 mirror is installed following the collimating lens for filtering majority of the remaining pump and Stokes beam. Next, F1 and F2 are used filters for filtering the residual small part of beams. F2 blocks residual part of Stokes one while F1 merely allows produced beam of CARS signal. Finally, just CARS beam gets to the photodiode and the generated signal is delivered to the scope for detection before we automatically record it on PC.

Alignment

Spatial overlap

Because CARS experiment involves two nearly co-propagating laser beams, we need to spatially align these beams into a confocal point. In order to successfully overlap them, a specifically devised plate having a hole is mounted onto both collimating and focussing lens as illustrated in Figure 3. Initially, 1064 nm Stokes beam needs to be aligned via the holes on the plate using beam walking technique. When that is accomplished, 708 nm pump beam is passed via both holes by the beam walking. Following that, pin hole with a 50 μm diameter is positioned on a movable stage at beam focus for ensuring the two beams are fully aligned at focal point. At first, 50 μm hole is modified in which the Stokes beam focuses. Next, the pump beam is passed via the pin hole. As a result, two beams are spatially intersected.

Temporal overlap

The temporal overlapping of the pulses is accomplished using different delay generators (Stanford Research Systems, Model DG535, USA). Two pulses are initiated employing 5 V output from IR laser through autonomously controlled delay generators. Generated pulses are uncovered using a photodiode and directed to oscilloscope (LeCoy, Wavepro 7300, USA) in which level of overlapping could be seen and controlled.

Data acquisition

A photodiode is used to identify produced signal as illustrated in Figure 3. We first observed on scope and then it is being logged on computer. In the measurement, the signal is attained using the photodiode and all data points are averaged before being saved. The dye laser is scanned around the anticipated peak to obtain the data. Once signal is detected, the data attained on the oscilloscope are logged on PC. Prior to examining the pump laser for recording the signal, as illustrated in Figure 2, the projected pump beam's peak wavelength is determined and then, the resultant wavelength of CARS signal is established.

RESULTS AND DISCUSSION

The parameters for experiment are needed to be optimized prior to carrying out the measurements. Firstly, dye laser and IR laser power outputs were improved to be adequately high in order to conduct the CARS experiment. The beam intensities are required to be roughly 10^{10} W cm^{-2} to accomplish the CARS measurement. Dye laser possessed 5 mJ pulse^{-1} output power and 10 ns pulse duration. Custom laser acquired 70 mJ pulse^{-1} output power and 140 ns pulse duration. The beam waist was evaluated to become 68 μm for pump and 46 μm for Stokes beam. Consequently, at focus, the pump and Stokes beam intensities were determined to be 5 x 10^{9} W cm^{-2} and 1 x 10^{10} W cm^{-2}. Additionally, 10% H_2 in Neon gas mixture was employed in the gas cell for carrying out the measurement.

Measured CARS signal

Initially S-branch transition in H_2 was investigated for measuring the CARS signal. The obtained signal of the S-branch transition in H_2 is demonstrated in Figure 4 at pressure of 600 torr. In this transition, the H_2 molecules at $v'' = 0, J'' = 1$ are promoted from to $v' = 1, J' = 3$. Between 708.800 and 709.000 nm, we scanned the pump laser in order to generate CARS signal meanwhile 1064.555 nm Stokes beam is being fixed. 0.005 nm step size was applied to dye laser during scanning stage for not skipping the resonant peak of the signal. 708.90 nm peak of CARS signal was obtained. Therefore, the resultant 531.370 nm CARS wavelength was measured which corresponds to green light.

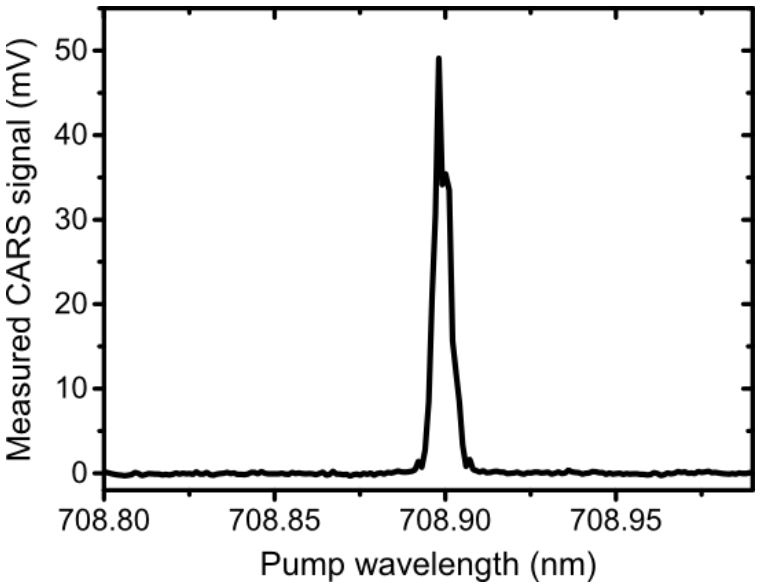

Figure 4. CARS signal of H_2 molecule for transition of S-branch is demonstrated. 708.899 nm pump and 1064.555 nm Stokes beam are employed. Resultant 531.370 nm wavelength of CARS signal is found.

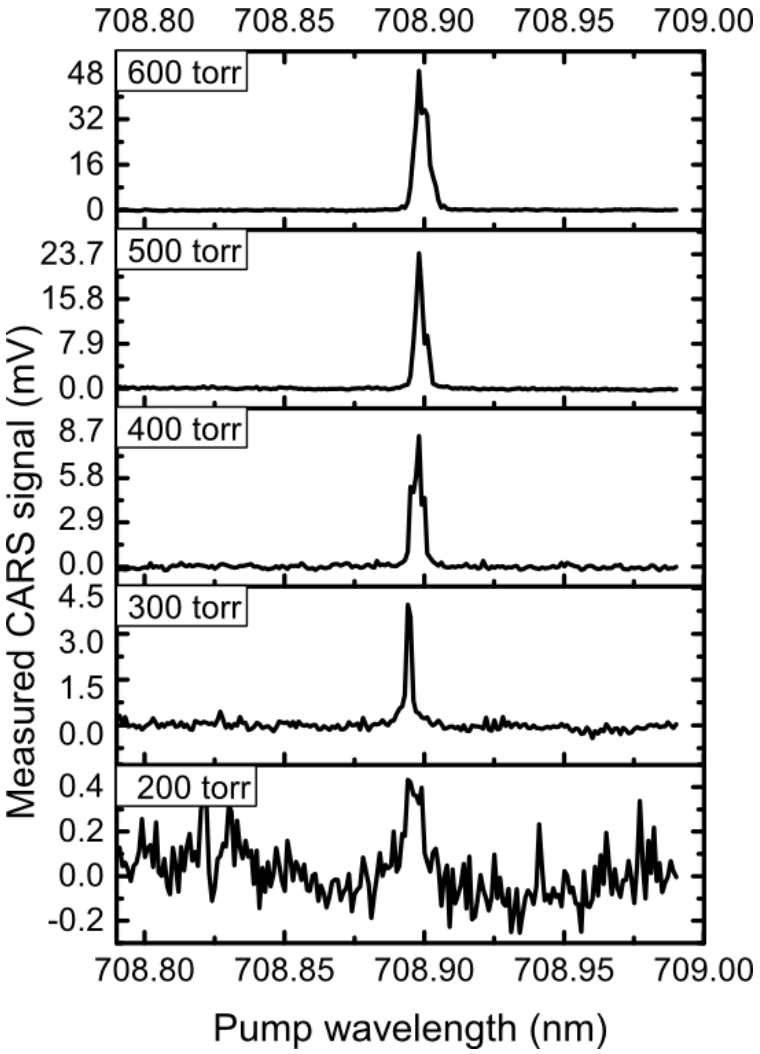

Figure 5. CARS signal with respect to various gas pressures in H_2 molecule for S-branch transition that differ from 200 to 600 torr.

CARS signal's pressure dependence

The signal's dependence on pressure measurement is conducted for determining the signal intensity on the pressure. Figure 5 indicates the dependence of CARS signal on pressure that is number density in interaction region. The measurement was performed for various pressures ranging between 200 and 600 torr. The signal rises with respect to increasing the molecules' number density as shown in Figure 5. Once pressure reaches to 200 torr, the signal practically vanishes. However, the CARS signal strength enhances dramatically by inserting additional amount of gas. A gas mix of 10% Hydrogen in Neon were utilized for measurements. Consequently, Hydrogen molecules produces a relative density of 10% in the gas mix.

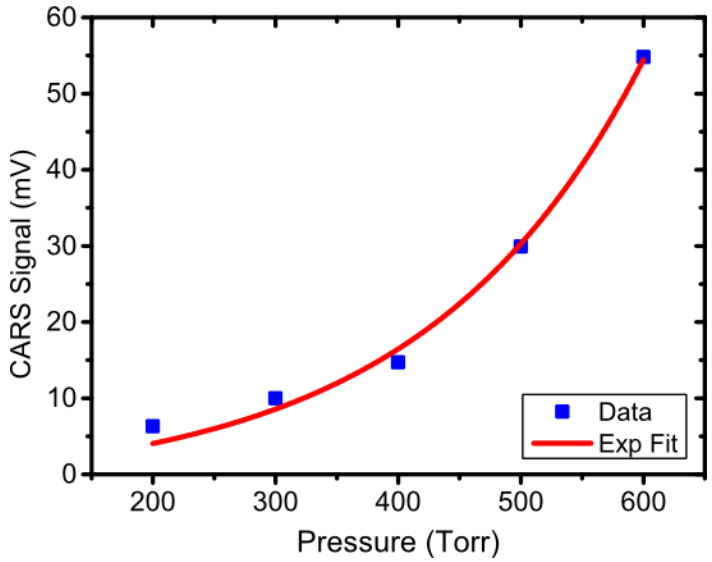

Figure 6. CARS signal of H_2 molecule for S-branch transition depending on various gas pressures that vary from 200 to 600 torr.

Table 1: Measured pressures with respect to obtained CARS signal.

Pressure (Torr)	**200**	**300**	**400**	**500**	**600**
CARS signal (mV)	7	10	15	30	55

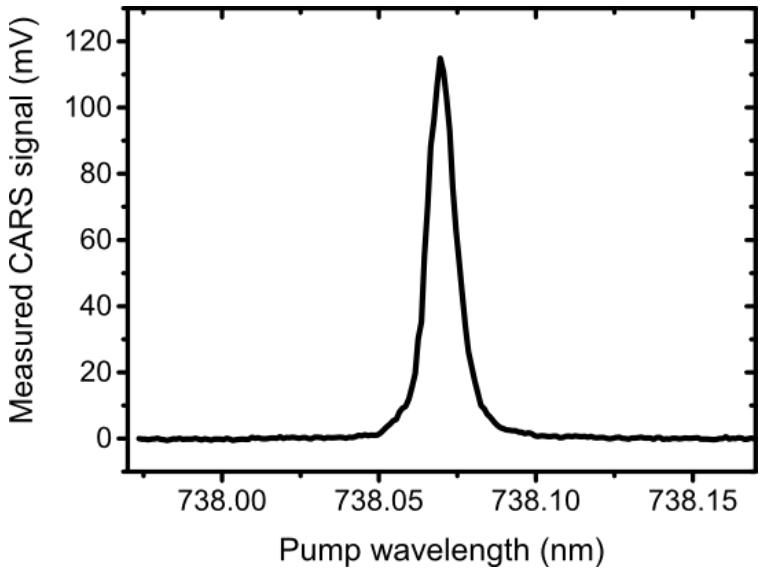

Figure 7. The enhanced CARS signal for transition of Q-branch in H_2 is demonstrated. 738.070 nm pump beam wavelength occurs as 1064.555 nm Stokes beam is fixed. Thus, subsequent 564.840 nm CARS signal is generated.

Figure 6 demonstrates CARS signal at various gas pressures. These data are fitted to a function (i.e. an exponential) on the Origin lab program. The signal grows exponentially while the pressure increases in the measurements. Hence, an agreement between our data and CARS theory has been achieved.

Q-branch transition measurement

An enhanced CARS signal is generated by investigating Q-branch transition of the H_2. The Q-branch signal strength is measured to be significantly enhanced compared to the preliminary measurements of the S-branch since Q-branch transition probability is much bigger than S-branch. In the Q-branch transition measurement, H_2 molecules at $v'' = 0, J'' = 1$ are excited to $v' = 1, J' = 1$. The signal of Q-branch transition is shown in Figure 7. Pump has a peak of 738.070 nm whereas it is 1064.555 nm for Stokes beam. Therefore, resultant beam has a peak at 564.840 nm that happens to be in the green region of the solar spectrum. In our measurement, the produced CARS signal is so intense that it could be observed by naked eyes. The fact that CARS signal could be viewed by naked eyes implies a substantial rise in the H_2 molecules' numbers being promoted to excited vibrational state $v' = 1$.

CONCLUSION

The wavelength of pump to be utilized in the SRP was successfully establish. Measurements of CARS experiment are effectively carried out for transitions of S- and Q-branch in H_2. On one hand, the wavelength of pump was established to be used in projected SRP on the other hand, we validated the laser setup is feasible for generating H_2 molecules at $v' = 1$ quantum state.

Even though we evaluated the CARS signal of H_2 S- and Q-branches in the measurements, the O-branch of H_2 transition can be identified using the same procedure as well. Moreover, CARS experiment could be utilized to ascertain the temperature of the molecule by establishing a number of rovibrational level populations of a molecule. The constraint in CARS method is that it is not very effective at low number densities since its efficiency is exceedingly reliant on the molecules' number density.

CARS spectroscopy has become a well-established method. Many experiments are described on establishing of the gas, rotational and vibrational temperatures of H_2 molecules in discharge plasmas (Dedic et al, 2017; Lempert & Adamovich, 2014; Shirley & Hall, 1977; Yatom et al, 2013) including concentration measurement (Jensen et al, 2019; Kearney et al, 2013; Ran et al, 2019; Regnier et al, 1974) by utilizing CARS method. CARS has similarly been employed in part to accomplish for preparing the oriented and aligned H_2 and HD molecules using stimulated Raman pumping(Bartlett et al, 2008; Choi et al, 2019; Folick et al, 2011; Lim et al, 2020). CARS method has recently been applied in Raman microspectroscopy for both in-vivo and in-vitro tissue diagnostics(Gong et al, 2020; Krafft et al, 2012; Moura et al, 2016). CARS has a significant potential in bioanalytical and biomedical sciences because of its non-invasive and label-free nature.

ACKNOWLEDGEMENTS

This research was supported by Turkish Ministry of National Education via a scholarship. I would like to thank University College London (UCL) for making this research possible through its research facilities.

Conflict of Interest

I declare that there is no conflict of interest during the planning, execution and writing of the article.

Author's Contiıbutions

I hereby declare that the planning, execution and writing of the article was done by me as the sole author of the article.

REFERENCES

Anderson A, 1971. The Raman Effect. Principles and Applications. Marcel Dekker: New York, 1973, 1-4.

Ando M, Kawano M, Tashiro A, Takamuku T, Shirota H, 2020. Low-Frequency Spectra of 1-Methyl-3-octylimidazolium Tetrafluoroborate Mixtures with Methanol, Acetonitrile, and Dimethyl Sulfoxide: A Combined Study of Femtosecond Raman-Induced Kerr Effect Spectroscopy and Molecular Dynamics Simulations. The Journal of Physical Chemistry B, 124(36): 7857-7871.

Babenko V, Bunkin N, Sychev A, 2020. Role of gas nanobubbles in nonlinear hyper-Raman scattering of light in water. JOSA B, 37(9): 2805-2814.

Bartlett NC, Miller DJ, Zare RN, Sofikitis D, Peter Rakitzis T, Alexander AJ, 2008. Preparation of oriented and aligned H 2 and HD by stimulated Raman pumping. The Journal of chemical physics, 129(8): 084312.

Begley R, Harvey A, Byer RL, 1974. Coherent anti-Stokes Raman spectroscopy. Applied Physics Letters, 25(7): 387-390.

Buric MP, Chen KP, Falk J, Woodruff SD, 2009. Improved sensitivity gas detection by spontaneous Raman scattering. Applied Optics, 48(22): 4424-4429.

Butler HJ, Ashton L, Bird B, Cinque G, Curtis K, Dorney J, Esmonde-White K, Fullwood NJ, Gardner B, Martin-Hirsch PL, 2016. Using Raman spectroscopy to characterize biological materials. Nature protocols, 11(4): 664-687.

Candan I, 2016. Production and measurement of H2 in rovibrationally excited states. UCL (University College London).

Choi DS, Kim CH, Lee T, Nah S, Rhee H, Cho M, 2019. Vibrational spectroscopy and imaging with non-resonant coherent anti-Stokes Raman scattering: double stimulated Raman scattering scheme. Optics express, 27(16): 23558-23575.

Christensen D, Rüther A, Kochan K, Pérez-Guaita D, Wood B, 2019. Whole-organism analysis by vibrational spectroscopy. Annual Review of Analytical Chemistry, 12: 89-108.

Coppendale N, Wang L, Douglas P, Barker P, 2011. A high-energy, chirped laser system for optical Stark deceleration. Applied Physics B, 104(3): 569.

Cutler AD, Gallo EC, Cantu LM, Rockwell RD, Goyne CP, 2018. Coherent anti-Stokes Raman spectroscopy of a premixed ethylene–air flame in a dual-mode scramjet. Combustion and Flame, 189: 92-105.

Dabrowski I, 1984. The Lyman and Werner bands of H2. Canadian Journal of Physics, 62(12): 1639-1664.

Dedic CE, Meyer TR, Michael JB, 2017. Single-shot ultrafast coherent anti-Stokes Raman scattering of vibrational/rotational nonequilibrium. Optica, 4(5): 563-570.

Eckbreth AC, 1996. Laser diagnostics for combustion temperature and species, *3*CRC press.

Eesley GL, 2013. Coherent Raman Spectroscopy, Elsevier.

Ehn A, Zhu J, Li X, Kiefer J, 2017. Advanced laser-based techniques for gas-phase diagnostics in combustion and aerospace engineering. Applied spectroscopy, 71(3): 341-366.

El-Diasty F, 2011. Coherent anti-Stokes Raman scattering: Spectroscopy and microscopy. Vibrational Spectroscopy, 55(1): 1-37.

Farahani, MA, Gogolla T, 1999. Spontaneous Raman scattering in optical fibers with modulated probe light for distributed temperature Raman remote sensing. Journal of Lightwave Technology, 17(8): 1379.

Folick A, Min W, Wang MC, 2011. Label-free imaging of lipid dynamics using Coherent Anti-stokes Raman Scattering (CARS) and Stimulated Raman Scattering (SRS) microscopy. Current opinion in genetics & development, 21(5): 585-590.

Gong L, Zheng W, Ma Y, Huang Z, 2020. Higher-order coherent anti-Stokes Raman scattering microscopy realizes label-free super-resolution vibrational imaging. Nature Photonics, 14(2): 115-122.

Goodhead RM, Moger J, Galloway TS, Tyler CR, 2015. Tracing engineered nanomaterials in biological tissues using coherent anti-Stokes Raman scattering (CARS) microscopy–a critical review. Nanotoxicology, 9(7): 928-939.

Harvey A, Nibler J, 1978. Coherent anti-Stokes Raman spectroscopy of gases. Applied Spectroscopy Reviews, 14(1): 101-143.

Heiman D, Hellwarth R, Levenson M, Martin G, 1976. Raman-induced Kerr effect. Physical Review Letters, 36(4): 189.

Jensen BB, Glover ZJ, Pedersen SM, Andersen U, Duelund L, Brewer JR, 2019. Label free noninvasive spatially resolved NaCl concentration measurements using Coherent Anti-Stokes Raman Scattering microscopy applied to butter. Food chemistry, 297: 124881.

Jiang H, Xu W, Ding Y, Chen Q, 2020. Quantitative analysis of yeast fermentation process using Raman spectroscopy: Comparison of CARS and VCPA for variable selection. Spectrochimica Acta Part A: Molecular and Biomolecular Spectroscopy, 228: 117781.

Jones RR, Hooper DC, Zhang L, Wolverson D, Valev VK, 2019. Raman techniques: Fundamentals and frontiers. Nanoscale research letters, 14(1): 1-34.

Kakinuma S, Shirota H, 2018. Femtosecond Raman-induced Kerr effect study of temperature-dependent intermolecular dynamics in molten bis (trifluoromethylsulfonyl) amide salts: effects of cation species. The Journal of Physical Chemistry B, 122(22): 6033-6047.

Kearney SP, Scoglietti DJ, Kliewer CJ, 2013. Hybrid femtosecond/picosecond rotational coherent anti-Stokes Raman scattering temperature and concentration measurements using two different picosecond-duration probes. Optics express, 21(10): 12327-12339.

Kiefer W, Bernstein H, 1972. The resonance Raman effect of the permanganate and chromate ions. Molecular Physics, 23(5): 835-851.

Kifer W, 1980. Active Raman spectroscopy: high resolution molecular spectroscopical methods. Journal of Molecular Structure, 59: 305-319.

Kliewer C, Bohlin A, Nordström E, Patterson B, Bengtsson PE, Settersten T, 2012. Time-domain measurements of S-branch N 2–N 2 Raman linewidths using picosecond pure rotational coherent anti-Stokes Raman spectroscopy. Applied Physics B, 108(2): 419-426.

Krafft C, Dietzek B, Popp J, Schmitt M, 2012. Raman and coherent anti-Stokes Raman scattering microspectroscopy for biomedical applications. Journal of biomedical optics, 17(4): 040801.

Kushwaha AS, Kumar A, Kumar R, Srivastava S, 2018. A study of surface plasmon resonance (SPR) based biosensor with improved sensitivity. Photonics and Nanostructures-Fundamentals and Applications, 31: 99-106.

Lempert WR, Adamovich IV, 2014. Coherent anti-Stokes Raman scattering and spontaneous Raman scattering diagnostics of nonequilibrium plasmas and flows. Journal of Physics D: Applied Physics, 47(43): 433001.

Lim S, Choi DS, Rhee H, Cho M, 2020. An Efficient Switching-Off of Coherent Anti-Stokes Raman Scattering via Double Stimulated Raman Scattering Processes of Heteromolecular Vibrational Modes. The Journal of Physical Chemistry B, 124(17): 3583-3590.

Liu CH, Zhou Y, Sun Y, Li J, Zhou L, Boydston-White S, Masilamani V, Zhu K, Pu Y, Alfano R, 2013. Resonance Raman and Raman spectroscopy for breast cancer detection. Technology in cancer research & treatment, 12(4): 371-382.

Madzharova F, Heiner Z, Kneipp J, 2017. Surface enhanced hyper Raman scattering (SEHRS) and its applications. Chemical Society Reviews, 46(13): 3980-3999.

Maher-McWilliams C, Douglas P, Barker P, 2012. Laser-driven acceleration of neutral particles. Nature Photonics, 6(6): 386-390.

Maker P, Terhune R, 1965. Study of optical effects due to an induced polarization third order in the electric field strength. Physical Review, 137(3A): A801.

Moura CC, Tare RS, Oreffo RO, Mahajan S, 2016. Raman spectroscopy and coherent anti-Stokes Raman scattering imaging: prospective tools for monitoring skeletal cells and skeletal regeneration. Journal of The Royal Society Interface, 13(118): 20160182.

Ochkin VN, 2009. Spectroscopy of low temperature plasma. John Wiley & Sons.

Portnov A, Bar I, Rosenwaks S, 2010. Highly sensitive standoff detection of explosives via backward coherent anti-Stokes Raman scattering. Applied Physics B, 98(2): 529-535.

Ran Y, Junghanns M, Boden A, Nolte S, Tünnermann A, Ackermann R, 2019. Temperature and gas concentration measurements with vibrational ultra-broadband two-beam femtosecond/picosecond coherent anti-Stokes Raman scattering and spontaneous Raman scattering. Journal of Raman Spectroscopy, 50(9): 1268-1275.

Regnier P, Moya F, Taran J, 1974. Gas concentration measurement by coherent Raman anti-Stokes scattering. AIAA Journal, 12(6): 826-831.

Saito R, Grüneis A, Samsonidze GG, Brar V, Dresselhaus G, Dresselhaus M, Jorio A, Cançado L, Fantini C, Pimenta M, 2003. Double resonance Raman spectroscopy of single-wall carbon nanotubes. New Journal of Physics, 5(1): 157.

Sarri B, Chen X, Canonge R, Grégoire S, Formanek F, Galey JB, Potter A, Bornschlögl T, Rigneault H, 2019. In vivo quantitative molecular absorption of glycerol in human skin using coherent anti-Stokes Raman scattering (CARS) and two-photon auto-fluorescence. Journal of Controlled Release, 308: 190-196.

Shirley J, Hall R, 1977. Vibrational excitation in H2 and D2 electric discharges. The Journal of Chemical Physics, 67(6): 2419-2421.

Short L, Thoms AV, Cao B, Sinyukov AM, Joshi A, Scully R, Sanders V, Voronine DV, 2015. Facile residue analysis of recent and prehistoric cook stones using handheld Raman spectrometry. Journal of Raman Spectroscopy, 46(1): 126-132.

Takaya T, Enokida I, Furukawa Y, Iwata K, 2019. Direct Observation of Structure and Dynamics of Photogenerated Charge Carriers in Poly (3-hexylthiophene) Films by Femtosecond Time-Resolved Near-IR Inverse Raman Spectroscopy. Molecules, 24(3): 431.

Tang Y, He C, Zheng X, Chen X, Gao T, 2020. Super-capacity information-carrying systems encoded with spontaneous Raman scattering. Chemical Science, 11(11): 3096-3103.

Teramoto Y, Ono R, 2014. Measurement of vibrationally excited N2 (v) in an atmospheric-pressure air pulsed corona discharge using coherent anti-Stokes Raman scattering. Journal of Applied Physics, 116(7): 073302.

Terhune R, Maker P, 1963. Nonlinear optics. Bull. Am. Phys. Soc, 8(359): 0003-0503.

Tolles WM, Nibler J, McDonald J, Harvey A, 1977. A review of the theory and application of coherent anti-Stokes Raman spectroscopy (CARS). Applied Spectroscopy, 31(4): 253-271.

Turner J, Kirby-Docken K, Dalgarno A, 1977. The quadrupole vibration-rotation transition probabilities of molecular hydrogen. The Astrophysical Journal Supplement Series, 35: 281.

Verdieck J, Peterson S, Savage C, Maker PD, 1970. Hyper-raman spectra of methane, ethane and ethylene in gas phase. Chemical Physics Letters, 7(2): 219-222.

Xie L, Ling X, Fang Y, Zhang J, Liu Z, 2009. Graphene as a substrate to suppress fluorescence in resonance Raman spectroscopy. Journal of the American Chemical Society, 131(29): 9890-9891.

Yan M, Zhang L, Hao Q, Shen X, Qian X, Chen H, Ren X, Zeng H, 2018. Surface-Enhanced Dual-Comb Coherent Raman Spectroscopy with Nanoporous Gold Films. Laser & Photonics Reviews, 12(9): 1800096.

Yang K, Wu Y, Jiang J, Ye P, Huang K, Hao Q, Zeng H, 2018. Fiber optical parametric oscillator and amplifier for CARS spectroscopy. IEEE Photonics Technology Letters, 30(10): 967-970.

Yatom S, Tskhai S, Krasik YE, 2013. Electric field in a plasma channel in a high-pressure nanosecond discharge in hydrogen: A coherent anti-stokes Raman scattering study. Physical review letters, 111(25): 255001.

Yeung, E. S. (1974) Inverse Raman effect: A quantitative spectroscopic technique. Journal of Molecular Spectroscopy, 53(3): 379-392.

Zhang C, Cheng JX, 2018. Perspective: Coherent Raman scattering microscopy, the future is bright. APL Photonics, 3(9): 090901.

Zheltikov A, 2000. Coherent anti-Stokes Raman scattering: from proof-of-the-principle experiments to femtosecond CARS and higher order wave-mixing generalizations. Journal of Raman Spectroscopy, 31(8-9): 653-667.

Zhu S, Fan C, Ding P, Liang E, Hou H, Wu Y, 2018. Theoretical investigation of a plasmonic substrate with multi-resonance for surface enhanced hyper-Raman scattering. Scientific reports, 8(1): 1-7.